Constitutive activation of B-Raf in the mouse germ line provides a model for human cardio-facio-cutaneous syndrome

Jelena Urosevic[a,1], Vincent Sauzeau[b,2], María L. Soto-Montenegro[c], Santiago Reig[c], Manuel Desco[c,d], Emma M. Burkitt Wright[e], Marta Cañamero[f], Francisca Mulero[f], Sagrario Ortega[f], Xosé R. Bustelo[b], and Mariano Barbacid[a,3]

[a]Molecular Oncology Program, Centro Nacional de Investigaciones Oncológicas (CNIO), E-28029 Madrid, Spain; [b]Centro de Investigación del Cáncer and Instituto de Biología Molecular y Celular del Cáncer, Consejo Superior de Investigaciones Cientificas-University of Salamanca, E-37007 Salamanca, Spain; [c]Unidad de Medicina y Cirugía Experimental, Hospital General Universitario "Gregorio Marañón," Centro de Investigación Biomédica en Red de Salud Mental (CIBERSAM), E-28007 Madrid, Spain; [d]Departamento de Bioingeniería e Ingeniería Aerospacial, Universidad Carlos III, E-28991 Madrid, Spain; [e]Genetic Medicine, University of Manchester, Manchester Academic Health Science Centre, Central Manchester University Hospitals National Health Service Foundation Trust, St. Mary's Hospital, Manchester M13 9WL, United Kingdom; and [f]Biotechnology Program, Centro Nacional de Investigaciones Oncológicas (CNIO), E-28029 Madrid, Spain

Edited* by Neal G. Copeland, Institute of Molecular and Cell Biology, Proteos, Singapore, and approved February 11, 2011 (received for review November 11, 2010)

RASopathies are a class of developmental syndromes that result from congenital mutations in key elements of the RAS/RAF/MEK signaling pathway. A well-recognized RASopathy is the cardio-facio-cutaneous (CFC) syndrome characterized by a distinctive facial appearance, heart defects, and mental retardation. Clinically diagnosed CFC patients carry germ-line mutations in four different genes, B-*RAF*, *MEK1*, *MEK2*, and K-*RAS*. B-*RAF* is by far the most commonly mutated locus, displaying mutations that most often result in constitutive activation of the B-RAF kinase. Here, we describe a mouse model for CFC generated by germ-line expression of a B-*Raf*^{LSLV600E} allele. This targeted allele allows low levels of expression of B-Raf^{V600E}, a constitutively active B-Raf kinase first identified in human melanoma. B-Raf$^{+/LSLV600E}$ mice are viable and display several of the characteristic features observed in CFC patients, including reduced life span, small size, facial dysmorphism, cardiomegaly, and epileptic seizures. These mice also show up-regulation of specific catecholamines and cataracts, two features detected in a low percentage of CFC patients. In addition, B-Raf$^{+/LSLV600E}$ mice develop neuroendocrine tumors, a pathology not observed in CFC patients. These mice may provide a means of better understanding the pathophysiology of at least some of the clinical features present in CFC patients. Moreover, they may serve as a tool to evaluate the potential therapeutic efficacy of B-RAF inhibitors and establish the precise window at which they could be effective against this congenital syndrome.

B-Raf signaling | developmental defects | chromaffin-derived tumor

Oncogenic mutations in the B-*RAF* locus have been found in a variety of human tumors (1, 2), with a single miscoding mutation, V600E, accounting for more than 80% of the B-*RAF* mutations identified to date (1, 3). Miscoding mutations in the B-*RAF* locus have also been observed in the germ line of patients with cardio-facio-cutaneous (CFC) syndrome, a congenital disorder that shares overlapping defects with other RASopathies such as Noonan, Costello, LEOPARD, and Legius syndromes as well as neurofibromatosis type I (4–8). All of these syndromes result from constitutive hyperactivation of the RAS/RAF/MEK/ERK signaling cascade, but they display unique characteristic features (8). CFC is characterized by craniofacial defects, short stature, cardiomegaly, ectodermal abnormalities, mental retardation, and neurological defects (9). About 75% of the patients molecularly diagnosed with CFC carry germ-line mutations in B-*RAF* (4, 5, 10). The rest display germ-line mutations in other components of the pathway, including K-*RAS*, *MEK1*, and *MEK2* (4, 11, 12). B-*RAF* mutations in CFC patients are widely distributed across the coding sequences, and most are predicted to result in hyperactivation of the B-RAF kinase. However, these mutations cause more limited activation of the downstream MEK/ERK kinases than those observed in human tumors, particularly those carrying the V600E mutation. In addition, some CFC patients carry B-RAF kinase-impairing mutations (3–5) that may activate the pathway by indirect mechanisms, possibly activating the related c-RAF kinase (13). Finally, some CFC-associated mutations have previously been identified in tumors (4–6), a feature also observed in patients with Costello syndrome (14).

Here, we report the generation and phenotypic characterization of mice expressing a hypomorphic B-*Raf*^{V600E} allele that phenocopies some of the key developmental defects observed in CFC patients. These mice should provide a suitable model system to better understand the molecular bases for this congenital disease and assay the suitability of potential therapeutic strategies (15, 16).

Results

Mouse Model for Human CFC Syndrome. We have taken advantage of a mouse strain, B-*Raf*$^{+/LSLV600E}$, that expresses a hypomorphic B-*Raf*^{V600E} allele at 5–10% the levels of the WT counterpart as determined by quantitative RT-PCR analyses (Fig. S1). The kinase activity of the B-Raf^{V600E} oncoprotein has been shown to be about 10- to 50-fold higher than that of other mutated B-Raf proteins, including those responsible for the CFC syndrome (3–5), and it causes embryonic lethality when expressed during embryonic development in mice (17). Thus, the low levels of expression of the B-*Raf*^{LSLV600E} allele are likely to result in constitutive levels of B-Raf kinase activity similar to those present in CFC patients (*Limited Life Span, Size, and Fertility in B-Raf*$^{+/LSLV600E}$ *Mice*).

To examine the status of the downstream Mek/Erk pathway in B-*Raf*$^{+/LSLV600E}$ mice, we performed Western blot analysis of cell extracts derived from adult heart and brain, two of the tissues displaying the most defects in B-*Raf*$^{+/LSLV600E}$ mice (*Limited Life*

Author contributions: J.U., V.S., X.R.B., and M.B. designed research; J.U., V.S., M.L.S.-M., S.R., and E.M.B.W. performed research; M.D., M.C., F.M., and S.O. analyzed data; J.U., E.M.B.W., X.R.B., and M.B. wrote the paper; M.D. and F.M. supervised imaging work; M.C. supervised histopathology work; and S.O. supervised the generation of the recombinant mice.

The authors declare no conflict of interest.

*This Direct Submission article had a prearranged editor.

[1]Present address: Oncology Programme, Institute for Research in Biomedicine (IRB), Parc Científic de Barcelona, E-08028 Barcelona, Spain.

[2]Present address: Institut de Recherche Thérapeutique (IRT-UN), L'institut du thorax-UMR915, 44007 Nantes Cedex 01, France.

[3]To whom correspondence should be addressed. E-mail: mbarbacid@cnio.es.

This article contains supporting information online at www.pnas.org/lookup/suppl/doi:10.1073/pnas.1016933108/-/DCSupplemental.

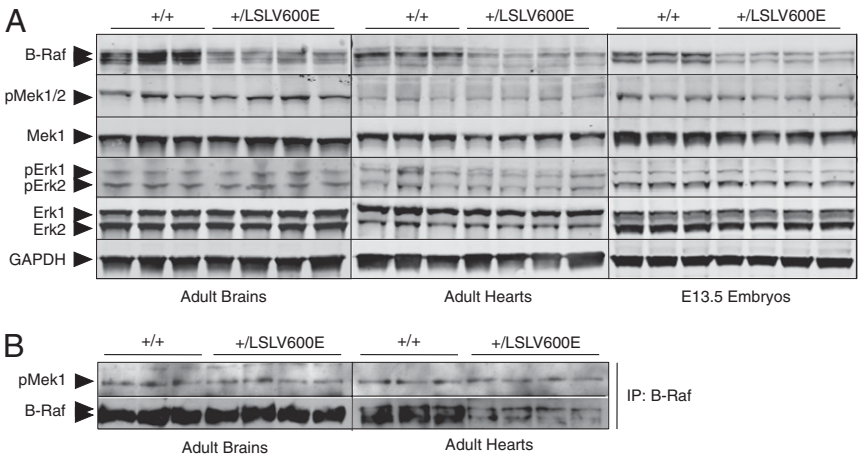

Fig. 1. Activation of the Mek/Erk pathway in B-*Raf*$^{+/LSLV600E}$ mice. (*A*) Protein extracts obtained from B-*Raf*$^{+/+}$ and B-*Raf*$^{+/LSLV600E}$ adult brain and heart tissues as well as E13.5 embryos were submitted to Western blot analyses using antibodies to B-Raf, pMek1/2, Mek1, pErk1/2, and Erk1/2. GAPDH was used as loading control. (*B*) Protein extracts obtained from B-*Raf*$^{+/+}$ and B-*Raf*$^{+/LSLV600E}$ adult brain and heart tissues were incubated with a monoclonal antibody against B-Raf, and the resulting immunoprecipitates were assayed for kinase activity using Mek1 as a substrate. The levels of pMek1 were determined by blotting with specific polyclonal antibodies against pMek1. The same membrane was used for Western blot analyses using B-Raf antibody as loading control. Arrowheads indicate the migration of the corresponding proteins.

Span, Size, and Fertility in B-Raf$^{+/LSLV600E}$ *Mice*). As illustrated in Fig. 1*A*, the levels of the B-Raf protein are about one-half of those observed in the corresponding tissues from WT littermates, thus indicating that the mutant B-Raf^{V600E} isoform must be expressed at low levels as indicated by RT-PCR analysis. Similar results were obtained with embryonic day (E)13.5 B-*Raf*$^{+/LSLV600E}$ embryos (Fig. 1*A*). Expression of the B-Raf^{V600E} isoform did not affect either the expression or phosphorylation levels of the downstream Mek and Erk proteins (Fig. 1*A*). Analysis of the overall B-Raf kinase activity in these mutant mice (that is, the kinase activity contributed by the normal B-Raf kinase and constitutive B-Raf^{V600E} hypomorphic isoform) did not increase, at least within the sensitivity levels of available in vitro kinase assays (Fig. 1*B*), thus suggesting that the activation of the Mek/Erk pathway in these mice must be subtle. These results are reminiscent of those previously obtained with a mouse model of Costello syndrome that expressed an endogenous H-Ras^{G12V} oncoprotein (18).

Limited Life Span, Size, and Fertility in B-*Raf*$^{+/LSLV600E}$ Mice. B-*Raf*$^{+/LSLV600E}$ mice were born at the expected Mendelian ratio, indicating that limited expression levels of B-Raf^{V600E} did not result in embryonic lethality. However, B-*Raf*$^{+/LSLV600E}$ mice showed reduced postnatal fitness, a defect highly dependent on their genetic makeup. Mice carrying the B-*Raf*^{V600E} allele in a mixed genetic background derived from C57BL/6J (75%) and 129Sv/J (25%) strains (designated as B6/129) displayed a bimodal survival curve characterized by death of 35% of the mice during their first 3 wk of life. Moreover, very few of these mice survived beyond 30 wk (Fig. 2*A*). This survival rate was further compromised when B6/129 B-*Raf*$^{+/LSLV600E}$ mice were backcrossed into the C57BL/6J background. Most mice carrying the B-*Raf*^{V600E} allele in a genetic background with a 98.5% contribution from C57BL/6J (designated as B6) died before they reached 12 wk of age (Fig. 2*A*). Conversely, survival increased when the B6 mice were crossed with CD1 females, an outbred strain (Fig. 2*A*). About 60% of the resulting progeny (designated as B6/CD1) survived more than 40 wk (Fig. 2*A*).

Histopathological analysis of tissues obtained from B-*Raf*$^{+/LSLV600E}$ mice that became sick during their first 3 wk of life revealed marked disorganization and atrophy of the thymus with increased numbers of apoptotic cells in the cortex and medulla as well as a reduction in the number of immature, terminal deoxynucleotidyl transferase (TdT)-positive thymocytes (Fig. S2). In addition, all tissues with lymphoid aggregates, such as the white pulp in spleen or gastrointestinal Peyer's patches, showed massive apoptosis (Fig. S3). Most of these animals displayed a reduction in the cytoplasm/nuclear ratio in most cells, although this phenotype was more evident in the kidney and in pancreatic acinar cells (Fig. S4). Finally, about one-half of the mice had reduced numbers and size of sebaceous glands in the skin and decreased white adipose tissue. None of these defects were observed in healthy animals of similar age. Moreover, they were present in all genetic backgrounds, albeit that they were more prevalent in the B6 mice.

All B-*Raf*$^{+/LSLV600E}$ mice, regardless of genetic background, displayed significant growth defects (Fig. 2*B*). They had reduced size and body weight at postnatal day 5 (P5), a phenotype that was further aggravated as the animals aged (Fig. 2*B* and Fig. S5). B-*Raf*$^{+/LSLV600E}$ mice also failed to mate. However, B-*Raf*$^{+/LSLV600E}$ males were not infertile, because their sperm efficiently fertilized WT oocytes in vitro. The contribution of the CD1 genetic background in B6/CD1 B-*Raf*$^{+/LSLV600E}$ males ameliorated mating defects, indicating that the breeding problems of B6 and

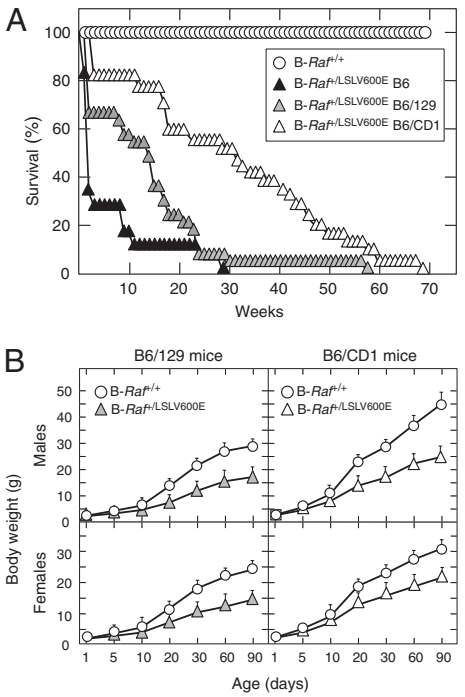

Fig. 2. B-*Raf*$^{+/LSLV600E}$ mice display decreased survival and growth rates. (*A*) Survival of B-*Raf*$^{+/+}$ mice of all genetic backgrounds (open circles; $n = 40$) and B-*Raf*$^{+/LSLV600E}$ mice of various genetic background including B6/CD1 (open triangles; $n = 44$), B6/129 (gray triangles; $n = 33$), and B6 (solid triangles; $n = 18$). (*B*) Body weights of B-*Raf*$^{+/+}$ male and female mice of B6/129 and B6/CD1 genetic backgrounds (open circles) compared with those of B-*Raf*$^{+/LSLV600E}$ male and female mice of B6/129 (gray triangles) and B6/CD1 (open triangles) genetic backgrounds. Error bars represent SEMs.

B6/129 mice were a consequence of their limited size and/or behavioral abnormalities.

B-*Raf*$^{+/LSLV600E}$ Mice Display Craniofacial Dysmorphism and Develop Cataracts. B-*Raf*$^{+/LSLV600E}$ mice, regardless of their genetic background, displayed more rounded and shorter heads as well as defects in the shape of their skull vault (Fig. 3). X-ray computed tomography (CT) analysis of 10-wk-old B6/129 B-*Raf*$^{+/LSLV600E}$ mice revealed significant differences in 6 of 10 cranial landmarks compared with WT siblings (Fig. 3*C*). The most significant deviations corresponded to the shape of frontal and parietal bones that form the skull vault. Milder but significant changes were also observed in the base of the cranium (Fig. 3). In addition, 40% of the B-*Raf*$^{+/LSLV600E}$ mice developed cataracts by 8 wk of age (Fig. S6). This percentage increased with time, with 80% of B-*Raf*$^{+/LSLV600E}$ mice being affected by 32 wk of age.

B-*Raf*$^{+/LSLV600E}$ Mice Develop Defects in Their Central and Autonomous Nervous Systems. B-*Raf*$^{+/LSLV600E}$ mice, regardless of genetic background and age, displayed marked hyperactivity characterized by an increased frequency of repetitive movements and locomotion. Despite these abnormalities, we did not observe alterations in locomotor coordination. The most prominent neurological alteration of these mice was the development of seizures, highly reminiscent of human tonic-clonic epilepsy (Movie S1). Seizures were first detected at 10–12 wk of age. The percentage of mice undergoing seizures increased progressively from 15% in 12-wk-old mice up to 50% in 20-wk-old animals (Fig. S7*A*). This percentage remained constant at later ages and did not seem to have an effect on mortality (Fig. S7*A*). Seizures normally appeared in response to routine handling and consisted of generalized convulsions that lasted 4–8 s (Movie S1). Seizure duration did not increase significantly with age (Fig. S7*B*). We also observed that 4-mo-old B-*Raf*$^{+/LSLV600E}$ mice had tachypnea and increased levels of noradrenaline, suggesting up-regulation of some sympathetic functions (Fig. S8).

Histopathological examination of B-*Raf*$^{+/LSLV600E}$ mice did not reveal major alterations in brain structure, regardless of the genetic background analyzed. Moreover, Nissl staining of the hippocampal area did not reveal gross differences in organization or neuron number. However, immunohistochemical staining for GFAP revealed significant increase in the number of

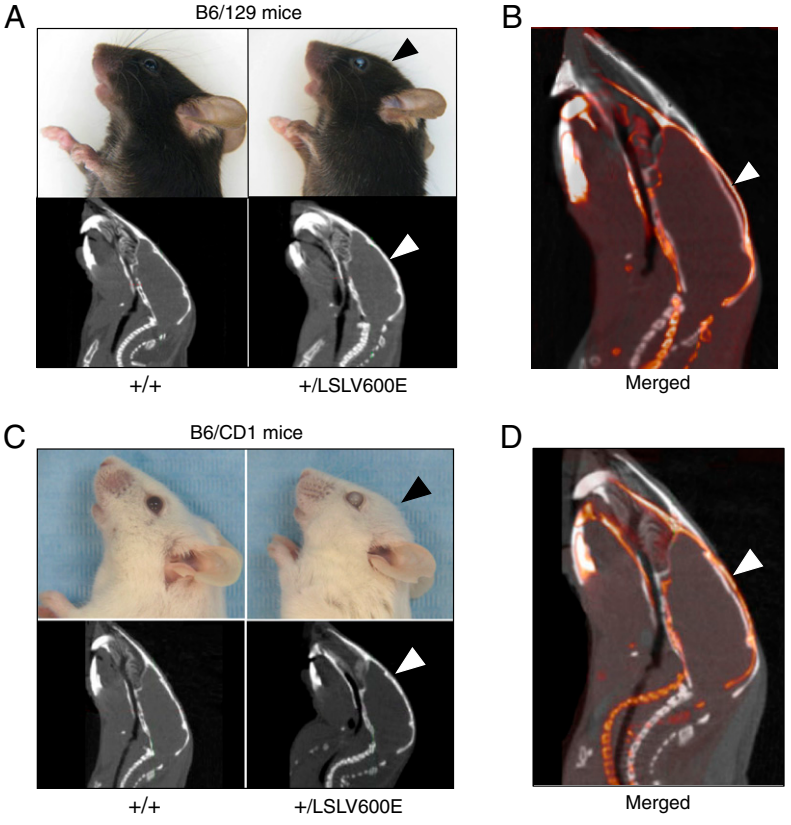

E

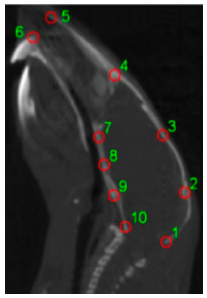

F

Landmark	Anatomical Position	Significance
1	Opisthion	0.0081
2	Intersection of interparietal and parietal bone	NS
3	Intersection of frontal and parietal bone	< 0.00001
4	Base of nasal bone	< 0.00001
5	Tip of nasal bone	NS
6	Center of alveolar ridge over maxillary incisor	0.0002
7	Spheno-ethmoid synchondrosis	NS
8	Spheno-occipital synchondrosis	NS
9	Intersphenoidal suture	0.0066
10	Basion	0.0028

Fig. 3. Cranial defects in B-*Raf*$^{+/LSLV600E}$ mice. (*A*) Representative side views of heads (*Upper*) and sagittal CT images (*Lower*) of adult B-*Raf*$^{+/+}$ and B-*Raf*$^{+/LSLV600E}$ mice in B6/129 genetic background illustrating the more rounded skull vault of the mutant mice (arrowheads). (*B*) Overlay of two representative sagittal CT sections of a B6/129 B-*Raf*$^{+/+}$ mouse (white) and a B6/129 B-*Raf*$^{+/LSLV600E}$ littermate (red). (*C*) Same as *A*, but images correspond to mice in a B6/CD1 genetic background. Note the cataracts in the eye of the two B-*Raf*$^{+/LSLV600E}$ mice. (*D*) Overlay of two representative sagittal CT sections of a B6/CD1 B-*Raf*$^{+/+}$ mouse (white) and a B6/CD1 B-*Raf*$^{+/LSLV600E}$ littermate (red). (*E*) 2D analysis of sagittal CT projections of 10-wk-old adult B-*Raf*$^{+/+}$ (n = 6) and B-*Raf*$^{+/LSLV600E}$ (n = 5) littermates (B6/129 genetic background). The anatomical position of a set of 10 homologous landmarks in a sagittal section of an adult B-*Raf*$^{+/+}$ mouse is indicated by red circles. (*F*) P values of differences between WT and mutant mice by Hotteling's T^2 test for each landmark coordinate (x and y) depicted in *E* after generalized procrustes superimposition. NS, not significant.

astrocytes in about 50% of adult B-*Raf*$^{+/LSLV600E}$ animals (Fig. 4). This increase in GFAP-positive cells was found to be independent of whether the mice had suffered seizures, thus suggesting that it was not a direct consequence of injuries caused by seizures (19, 20).

Heart and Kidney Defects in B-*Raf*$^{+/LSLV600E}$ Mice. Further examination of B-*Raf*$^{+/LSLV600E}$ mice indicated that they had increased heart/body weight ratios, regardless of their genetic background (Table S1). This defect was specific for hearts, because other viscera, such as liver or kidney, showed no significant size alterations (Table S1). The cardiomegaly of B-*Raf*$^{+/LSLV600E}$ mice was caused by an increase in the total number of cardiomyocytes rather than alterations in their size (Fig. 5 *C* and *D*). We did not observe gross alterations in the histological structure of auricles, ventricles, or aortic valves (Fig. 5*A*). Likewise, we did not detect any sign of tissue fibrosis (Fig. 5*B*).

We examined heart function in 2-mo-old B6/CD1 B-*Raf*$^{+/LSLV600E}$ mice by positron emission tomography (PET) analysis. These mice generated significantly lower end systolic and end diastolic volumes compared with WT littermates (Fig. 5 *E* and *F*). The heart ejection fractions were significantly increased in the mutant animals (Fig. 5*G*), but this did not affect their systolic arterial blood pressure (Table S1). Moreover, B-*Raf*$^{+/LSLV600}$ mice did not display arrhythmias or high blood pressure, regardless of their genetic background (Table S1). The absence of hypertension in these mutant mice is in agreement with the lack of heart fibrosis and cardiovascular remodeling. Finally, no major differences in renal morphology or histology were observed in these mutant mice. However, urine production and creatinine clearance in 2-mo-old B6 mice were significantly lower than in WT littermates, suggesting a possible deficiency in glomerular filtration (Table S1).

High Incidence of Chromaffin-Derived Tumors in B-*Raf*$^{+/LSLV600E}$ Mice. Expression of B-Raf^{V600E} in adult mice results in rapid development of lung adenomas and melanomas (21, 22). B6/CD1 B-*Raf*$^{+/LSLV600E}$ mice developed paragangliomas and pheochromocytomas with high frequency (20/25) and relatively short latency (about 5 mo) (Fig. 6). These tumor types are derived from chromaffin cells of the sympathetic/parasympathetic chain and adrenal gland medulla, respectively (23). Immunohistochemical staining with antibodies against chromogranin A and synaptophysin confirmed their neuroendocrine origin (Fig. 6*B*). Although these tumors were usually benign, 20% of the tumor-bearing mice (4 of 20) displayed metastasis to distant tissues, including stomach, pancreas, liver, or lung (Fig. 6*C*). A limited number of B6/CD1 B-*Raf*$^{+/LSLV600E}$ mice (10–20%) also developed lung adenomas (grades II–III) and melanocytic hyperplasia in the skin dermis (Fig. S9). We did not observe tumors in B6 or B6/129 B-*Raf*$^{+/LSLV600E}$ mice, with the exception of a single animal that carried a low-grade lung adenoma.

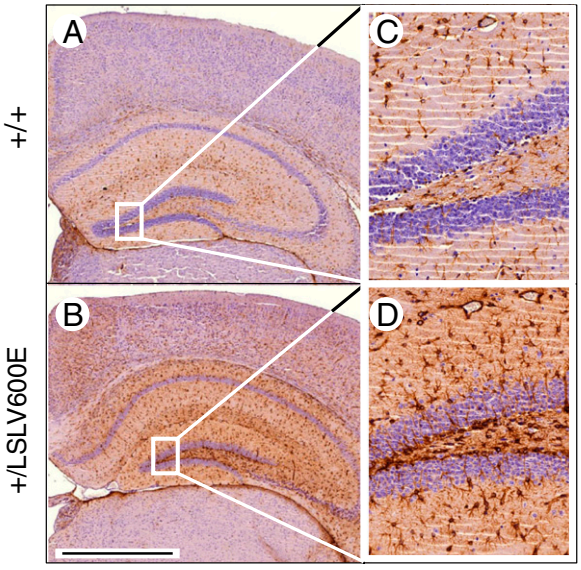

Fig. 4. Increased number of GFAP positive cells in hippocampal and cortical areas. (*A* and *B*) GFAP staining of hippocampal areas from 8-wk-old B-*Raf*$^{+/+}$ and B-*Raf*$^{+/LSLV600E}$ littermates (B6/CD1 background). (*C* and *D*) Amplified image of the quadrant indicated in *A* and *B*. (Scale bar, 1,000 μm.)

Discussion

A significant fraction of patients with CFC syndrome carry germline mutations in their B-*RAF* locus. These mutations are thought to result in constitutive activation of B-RAF kinase activity (3–5). Here, we have generated a mouse strain that expresses low levels of a constitutively active B-Raf^{V600E} kinase, hoping to mimic the limited but constitutive levels of B-RAF kinase activity present in patients with CFC syndrome. Indeed, B-*Raf*$^{+/LSLV600E}$ mice display similar, albeit not identical, defects to those found in CFC patients, including reduced life span, small size, facial dysmorphism, and epileptic seizures (9). These mice also show upregulation of specific catecholamines and cataracts, two features detected in a low percentage of CFC patients (11).

B-*Raf*$^{+/LSLV600E}$ mice display cardiomegaly because of an increased number of cardiomyocytes. Instead, the cardiomegaly observed in CFC patients is believed to be because of cardiomyocyte hypertrophy. However, there are no sufficient histological data to rule out the possibility that early onset cardiomyopathies with hypertrophic appearances could have increased cardiomyocyte numbers. B-*Raf*$^{+/LSLV600E}$ mice do not develop other cardiovascular defects typically present in CFC patients, such as pulmonary valve stenosis, septal defects, and aortic abnormalities (12, 24, 25). Whether these differences are caused by the intrinsic physiological differences between the cardiovascular systems of rodents and humans or differences in the constitutive B-Raf kinase activity remains to be determined. However, B-*Raf*$^{+/LSLV600E}$ mice display certain phenotypes not described in CFC patients, including tachypnea, thymic disorganization, increased brain astrocyte numbers, and development of neuroendocrine tumors such as pheochromocytomas and paragangliomas. It is possible that some of these defects may also appear in CFC patients but with sufficiently low penetration to have escaped detection thus far.

The main phenotypes present in B-*Raf*$^{+/LSLV600E}$ mice are independent of the genetic background. They include reduced size and body weight, craniofacial changes, cataracts, cardiomegaly, and epileptic seizures. These observations indicate that increased and/or constitutive B-Raf kinase activity triggers such defects without significant epistatic influence from other loci. In contrast, their postnatal lethality is clearly influenced by other ancillary genetic factors, because its severity depends on the genetic background. In addition, the development of chromaffin cell-derived tumors was also exclusively observed in the B6/CD1 genetic background. However, in this case, we cannot rule out that the absence of tumors in B6 and B6/129 backgrounds is because of the limited survival of these mice.

The phenotype of B-*Raf*$^{+/LSLV600E}$ animals shows limited overlap with that of mice carrying a constitutively active H-*Ras* oncogene in their germ line, a model for Costello syndrome (14). These strains develop similar facial dysmorphism and enlarged hearts (18, 26). However, unlike B-*Raf*$^{+/LSLV600E}$ mice, H-*Ras*$^{+/G12V}$ animals develop left ventricular hypertrophy, enlarged aortic valves, angiotensin II-dependent hypertension, extensive cardiovascular remodeling, and fibrosis in the heart and kidneys (18). Also, H-*Ras*$^{+/G12V}$ mice (even in homozygosity) do not display some of the defects present in B-*Raf*$^{+/LSLV600E}$ mice, such as small size, cataracts, and increased numbers of brain astrocytes or epileptic seizures (18, 26). These mouse strains also differ in their tumorigenic potential, because H-*Ras* mutant mice develop mammary hyperplasia (18) as well as papillomas and

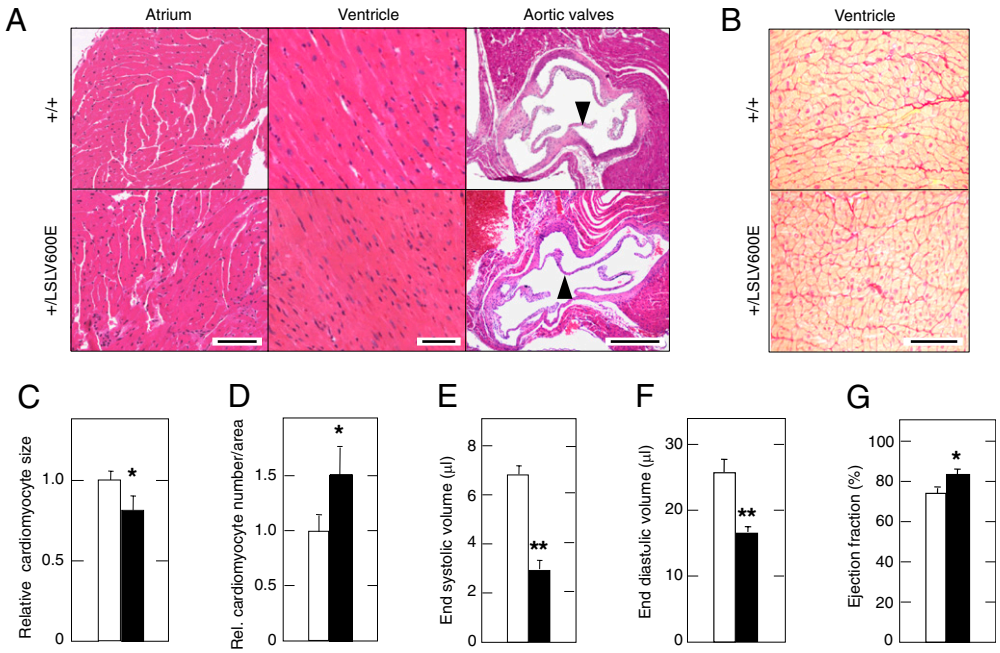

Fig. 5. Heart defects in B-*Raf*$^{+/LSLV600E}$ mice. (*A*) Histological analysis of heart chambers and aortic valves of 8-wk-old B-*Raf*$^{+/+}$ and B-*Raf*$^{+/LSLV600E}$ littermates. (*Left*) H&E staining of atrial cardiomyocytes. (Scale bar, 100 μm.) (*Center*) H&E staining of ventricular cardiomyocytes. (Scale bar, 50 μm.) (*Right*) H&E staining of aortic valves (arrowheads). (Scale bar, 500 μm.) (*B*) Sirius red staining of ventricular cardiomyocytes of B-*Raf*$^{+/+}$ and B-*Raf*$^{+/LSLV600E}$ littermates. (Scale bar, 100 μm.) (*C*) Relative cardiomyocyte size. (*D*) Relative number of cardiomyocytes per area. (*E–G*) PET analysis of heart functions including (*E*) end systolic volume, (*F*) end diastolic volume, and (*G*) ejection fraction. B-*Raf*$^{+/+}$ (open bars) and B-*Raf*$^{+/LSLV600E}$ (solid bards) mice (n = 6) had a B6 (*A–D*) or B6/CD1 (*E–G*) genetic background. For each mouse, three photos of the ventricular area were taken using the same magnification (20×). The number of cardiomyocytes was determined by counting the nuclei. The area occupied by the cardiomyocytes was determined using Image J software. Relative values represented in *C* and *D* were obtained by normalizing with those values obtained from control B-*Raf*$^{+/+}$ animals. Error bars represent SEMs. *$P < 0.05$; **$P < 0.01$.

angiosarcomas (26) but not neuroendocrine tumors. Limited overlapping defects have also been reported between human CFC and Costello syndromes (12).

Indeed, the defects observed in H-*RAS*–induced Costello syndrome and B-*RAF*–dependent CFC syndrome are difficult to explain based on our current knowledge of H-RAS and B-RAF signaling. In mice, it could be expected that H-*Ras*$^{+/G12V}$ animals would display a broader range of defects considering that H-Ras proteins signal through pathways not available to B-Raf, such as the PI3Kinase and the Ral-guanine nucleotide dissociation stimulator pathways. Moreover, H-*Ras*$^{+/G12V}$ mice express the oncogenic H-Ras^{G12V} protein at normal levels, whereas the B-*Raf*$^{+/LSLV600E}$ allele is only expressed at about 5–10% normal levels. Biochemical analysis of the Raf/Mek/Erk pathway in H-*Ras*$^{+/G12V}$ and B-*Raf*$^{+/LSLV600E}$ mice did not reveal significant alterations (this study and ref. 18), suggesting that the developmental defects induced by these mutations might be because of changes in signal intensity too subtle to be detected by standard biochemical methods. Alternatively, some of the observed differences may stem from the differential pattern of expression of

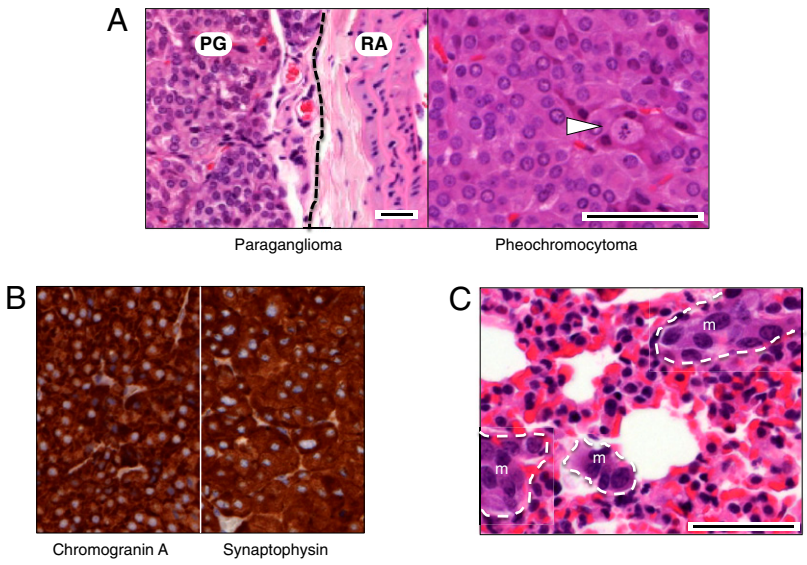

Fig. 6. B-*Raf*$^{+/LSLV600E}$ mice develop chromaffin cell tumors. (*A Left*) H&E staining of a representative paraganglioma (PG) located adjacent to the renal artery (RA). Dotted line serves to separate both structures. (*A Right*) A pheochromocytoma depicting a mitotic figure (arrowhead). (*B*) Immunohistochemical staining for chromogranin A and synaptophysin of a representative pheochromocytoma. (*C*) H&E staining of micrometastases (m) detected in the lung of a pheochromocytoma-bearing mouse. Note the difference in nuclear and cellular size between normal lung parenchyma and a group of cells forming micrometastases. (Scale bars, 50 μm.)

these proteins. For instance, the higher levels of expression of the B-*Raf* locus in the nervous system may account for the seizures and neuroendocrine tumors exclusively observed in the B-*Raf*$^{+/LSLV600E}$ animals. Full understanding of the molecular events responsible for the developmental defects observed in the various RASopathies (8) will require a more profound knowledge of how these proteins signal in vivo.

The B-*Raf*$^{+/LSLV600E}$ animals described here may help in understanding the pathophysiology of at least some of the clinical features present in CFC patients and possibly other RASopathies. Moreover, they could help to identify genetic factors that contribute to the pleiotropic manifestations of the clinical disorders by introducing the B-*Raf*^{LSLV600E} allele in different genetic backgrounds or combined with other alleles. Recently, MEK and fibroblast growth factor receptor 1 (FGFR1) inhibitors have been used to study development of zebra fish embryos carrying CFC mutations (27). Whereas prolonged treatments resulted in axis abnormalities, short exposure during specific developmental windows prevented these defects (27). More recently, B-RAF selective inhibitors have been developed and shown to have a significant antitumor effect in B-RAF^{V600E}–induced human melanomas (15, 16). The B-*Raf*$^{+/LSLV600E}$ strain could be a tool, not only to determine the therapeutic efficacy of these compounds in the treatment of CFC but as previously shown in zebra fish (27), to establish the precise window at which these inhibitors could be effectively used to treat this congenital syndrome.

Materials and Methods

Generation of Mice. The detailed strategy used to generate the B-*Raf*$^{+/LSLV600E}$ strain and genotype the corresponding alleles is described in *SI Materials and Methods*.

Western Blot and Kinase Assay. Protein extracts obtained from whole-mouse embryos (E13.5; 50 μg), adult heart (70 μg), and adult brain (50 μg) were fractionated in SDS/PAGE gels, transferred onto nitrocellulose membranes, and subjected to immunoblot analysis according to standard procedures (*SI Materials and Methods*).

Histopathology and Immunohistochemistry. Tissues were dissected, fixed in 10% buffered formalin (Sigma), and embedded in paraffin; 2- to 3-μm-thick sections were stained with H&E. Antibodies used for immunohistochemistry included those to synaptophysin (1:1; Dako), GFAP (1:25; Dako), chromogranin A (1:300; Abcam), active caspase 3 (1:20; R&D Systems), and terminal deoxynucleotidyl transferase (1:15; Dako). Heart sections were stained with Sirius Red (Fluka) to visualize fibrosis (28, 29).

Physiological Parameters. Blood pressure and heart rates were recorded in conscious mice with an automated multichannel system using the tail-cuff method and a photoelectric sensor (Niprem 546; Cibertec SA) (29, 30). Creatinine concentrations in urine and plasma were determined by a modification of Jaffé's reaction method (28, 29). Adrenaline and noradrenaline levels were determined by using CatCombi ELISA kit (IBL) following the manufacturer's instructions. For the determination of breathing activity, animals were lightly anesthetized with 1 g urethane/kg body weight. Forceps connected to a force transducer by a flexible wire were attached to the anesthetized mice at the diaphragm level. Respiratory amplitude and frequency were then collected using a digital data recorder (MacLab/4e; AD Instruments), and data were integrated with the Chart v3.4 software (AD Instruments).

CT and PET. Acquisition of CT and PET images was carried out according to standard protocols using an eXplore Vista PET CT (GE Healthcare). Morphometric analysis was carried out as described in *SI Materials and Methods*.

ACKNOWLEDGMENTS. We thank Isabel Hernandez and Carmen Guerra for their comments and Mayte Lamparero and Isabel Aragon for excellent technical assistance. We also value the excellent support provided by the Comparative Pathology and Transgenic Mice Core Units of the Centro Nacional de Investigaciones Oncológicas. Work in the laboratory of M.D. was funded by Consorcios Estratégicos Nacionales en Investigación Técnica Program (CDTEAM) Grant TEC2008-06715-C02-01, Centro de Investigación Biomédica en Red Program Grants CB06/01/0079 and PNSD 2007-2010, Fondo de Investigación Sanitaria (FIS) Grant CP08/00017, and Fundación de la Mutua Madrileña del Automovil (FMMA). E.M.B.W. was the holder of a United Kingdom National Institute for Health Research Academic Clinical Fellowship and was supported by the Manchester Biomedical Research Centre. Work in the laboratory of X.R.B. was funded by National Institutes of Health Grant R01CA073735, Spanish Ministry of Science and Innovation (MICINN) Grants SAF2009-07172 and RD06/0020/0001, Autonomous Government of Castilla y León (GR97), and Asociación Española contra el Cáncer. Work in the laboratory of M.B. was supported by European Union-Framework Programme Grants LSHG-CT-2006-037188 and LSHG-CT-2007-037665 (to M.B.), European Research Council Grant ERC-AG/250297-RAS AHEAD (to M.B.), MICINN Grants SAF2006-11773 and CSD2007-00017 (to M.B.), FMMA (to M.B.), FIS Grant PI042124, and Autonomous Community of Madrid Grant GR/SAL/0349/2004.

1. Davies H, et al. (2002) Mutations of the BRAF gene in human cancer. *Nature* 417: 949–954.
2. Wellbrock C, Karasarides M, Marais R (2004) The RAF proteins take centre stage. *Nat Rev Mol Cell Biol* 5:875–885.
3. Wan PT, et al. (2004) Mechanism of activation of the RAF-ERK signaling pathway by oncogenic mutations of B-RAF. *Cell* 116:855–867.
4. Niihori T, et al. (2006) Germline KRAS and BRAF mutations in cardio-facio-cutaneous syndrome. *Nat Genet* 38:294–296.
5. Rodriguez-Viciana P, et al. (2006) Germline mutations in genes within the MAPK pathway cause cardio-facio-cutaneous syndrome. *Science* 311:1287–1290.
6. Schubbert S, Shannon K, Bollag G (2007) Hyperactive Ras in developmental disorders and cancer. *Nat Rev Cancer* 7:295–308.
7. Brems H, et al. (2007) Germline loss-of-function mutations in SPRED1 cause a neurofibromatosis 1-like phenotype. *Nat Genet* 39:1120–1126.
8. Tidyman WE, Rauen KA (2009) The RASopathies: Developmental syndromes of Ras/MAPK pathway dysregulation. *Curr Opin Genet Dev* 19:230–236.
9. Roberts A, et al. (2006) The cardiofaciocutaneous syndrome. *J Med Genet* 43:833–842.
10. Rodriguez-Viciana P, Rauen KA (2008) Biochemical characterization of novel germline BRAF and MEK mutations in cardio-facio-cutaneous syndrome. *Methods Enzymol* 438: 277–289.
11. Gripp KW, et al. (2007) Further delineation of the phenotype resulting from BRAF or MEK1 germline mutations helps differentiate cardio-facio-cutaneous syndrome from Costello syndrome. *Am J Med Genet A* 143A:1472–1480.
12. Narumi Y, et al. (2007) Molecular and clinical characterization of cardio-facio-cutaneous (CFC) syndrome: Overlapping clinical manifestations with Costello syndrome. *Am J Med Genet A* 143A:799–807.
13. Heidorn SJ, et al. (2010) Kinase-dead BRAF and oncogenic RAS cooperate to drive tumor progression through CRAF. *Cell* 140:209–221.
14. Aoki Y, et al. (2005) Germline mutations in HRAS proto-oncogene cause Costello syndrome. *Nat Genet* 37:1038–1040.
15. Bollag G, et al. (2010) Clinical efficacy of a RAF inhibitor needs broad target blockade in BRAF-mutant melanoma. *Nature* 467:596–599.
16. Flaherty KT, et al. (2010) Inhibition of mutated, activated BRAF in metastatic melanoma. *N Engl J Med* 363:809–819.
17. Mercer K, et al. (2005) Expression of endogenous oncogenic V600EB-raf induces proliferation and developmental defects in mice and transformation of primary fibroblasts. *Cancer Res* 65:11493–11500.
18. Schuhmacher AJ, et al. (2008) A mouse model for Costello syndrome reveals an Ang II-mediated hypertensive condition. *J Clin Invest* 118:2169–2179.
19. Stringer JL (1996) Repeated seizures increase GFAP and vimentin in the hippocampus. *Brain Res* 717:147–153.
20. Pekny M, Nilsson M (2005) Astrocyte activation and reactive gliosis. *Glia* 50:427–434.
21. Dankort D, et al. (2007) A new mouse model to explore the initiation, progression, and therapy of BRAFV600E-induced lung tumors. *Genes Dev* 21:379–384.
22. Dhomen N, et al. (2009) Oncogenic Braf induces melanocyte senescence and melanoma in mice. *Cancer Cell* 15:294–303.
23. Bryant J, Farmer J, Kessler LJ, Townsend RR, Nathanson KL (2003) Pheochromocytoma: The expanding genetic differential diagnosis. *J Natl Cancer Inst* 95: 1196–1204.
24. Armour CM, Allanson JE (2008) Further delineation of cardio-facio-cutaneous syndrome: Clinical features of 38 individuals with proven mutations. *J Med Genet* 45: 249–254.
25. Nyström AM, et al. (2008) Noonan and cardio-facio-cutaneous syndromes: Two clinically and genetically overlapping disorders. *J Med Genet* 45:500–506.
26. Chen X, et al. (2009) Endogenous expression of Hras(G12V) induces developmental defects and neoplasms with copy number imbalances of the oncogene. *Proc Natl Acad Sci USA* 106:7979–7984.
27. Anastasaki C, Estep AL, Marais R, Rauen KA, Patton EE (2009) Kinase-activating and kinase-impaired cardio-facio-cutaneous syndrome alleles have activity during zebrafish development and are sensitive to small molecule inhibitors. *Hum Mol Genet* 18:2543–2554.
28. Sauzeau V, et al. (2006) Vav3 proto-oncogene deficiency leads to sympathetic hyperactivity and cardiovascular dysfunction. *Nat Med* 12:841–845.
29. Sauzeau V, Jerkic M, López-Novoa JM, Bustelo XR (2007) Loss of Vav2 proto-oncogene causes tachycardia and cardiovascular disease in mice. *Mol Biol Cell* 18:943–952.
30. Sauzeau V, Sevilla MA, Montero MJ, Bustelo XR (2010) The Rho/Rac exchange factor Vav2 controls nitric oxide-dependent responses in mouse vascular smooth muscle cells. *J Clin Invest* 120:315–330.